Structural Analysis of Amorphous Molecular Solid Using Infrared Multiple-Angle Incidence Resolution Spectrometry

赤外多角入射分解分光法によるアモルファス分子性固体の構造解析

〇Tetsuya Hama; Komaba Institute for Science, UTokyo
〇羽馬 哲也 (東大･先進科学研究機構)

Atsuki Ishibashi, Akira Kouchi, Naoki Watanabe;
Institute of Low Temperature Science, Hokkaido Univ.
石橋 篤季, 香内 晃, 渡部 直樹 (北大･低温研)

Nobutaka Shioya, Takafumi Shimoaka, and Takeshi Hasegawa;
Institute for Chemical Research, Kyoto Univ.
塩谷 暢貴, 下赤 卓史, 長谷川 健 (京大･化研)

Amorphous ice in space: building blocks for the planetary systems

IR observation toward interstellar clouds

Interstellar clouds
(10–100 K)

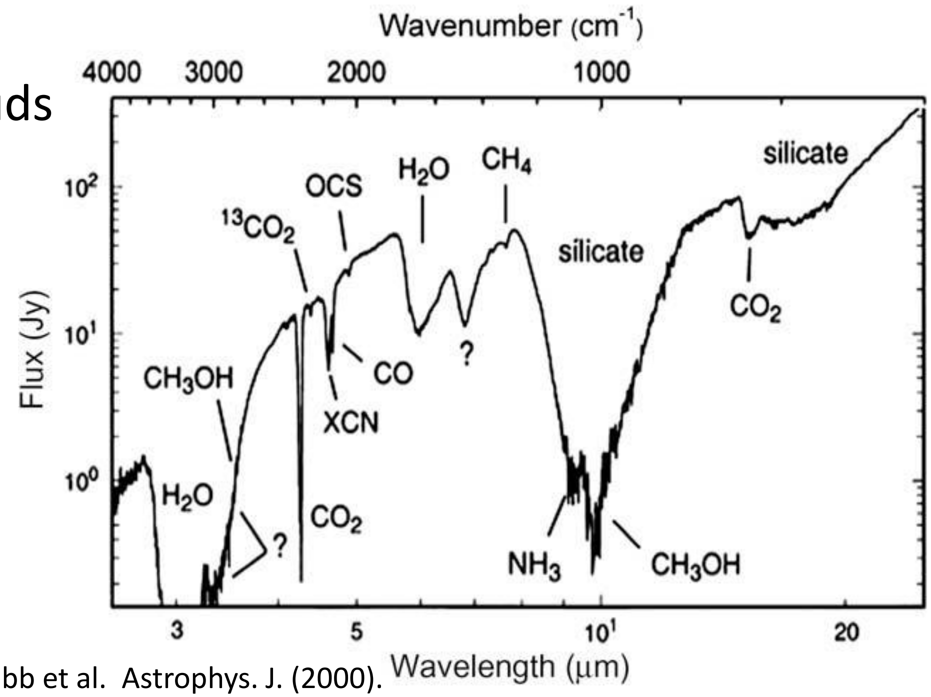

Gibb et al. Astrophys. J. (2000).

?

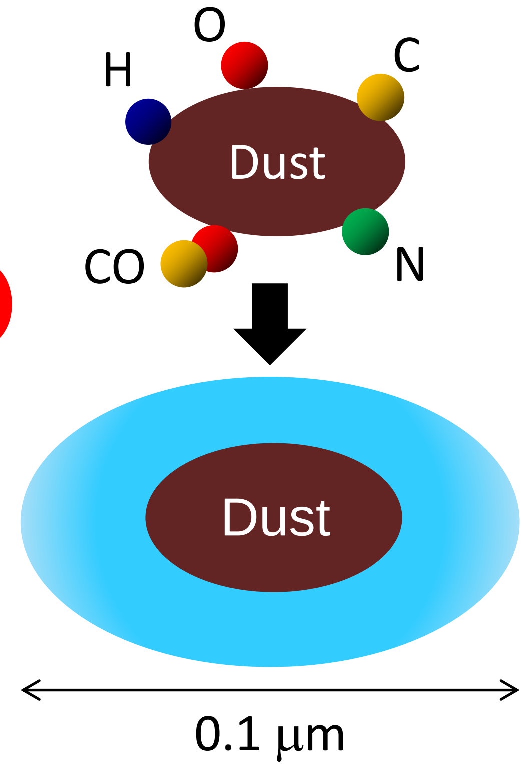

Silicate dust grains covered with amorphous H_2O ice (T_{cry}=140 K)

Similar chemical constituents to comets

Icy dust grains are the precursors of planetary material

Comets (icy bodies)

Earth

All solid species (except for CO) require dust surface reactions to attain the observed abundances.

Laboratory study for dust surface chemistry

Ultra-high vacuum chamber, 4 K cryostat, lasers, FT-IR, hydrogen atomic source etc…

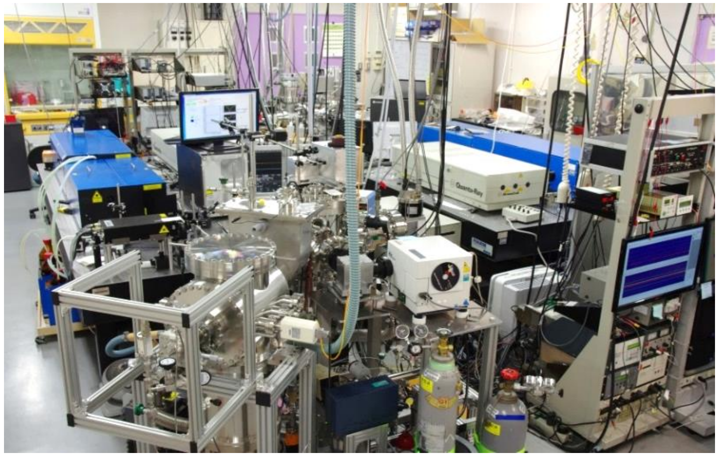

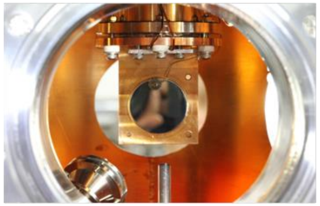

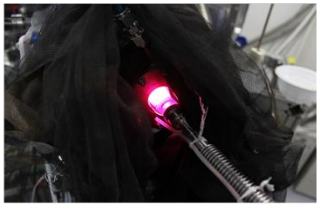

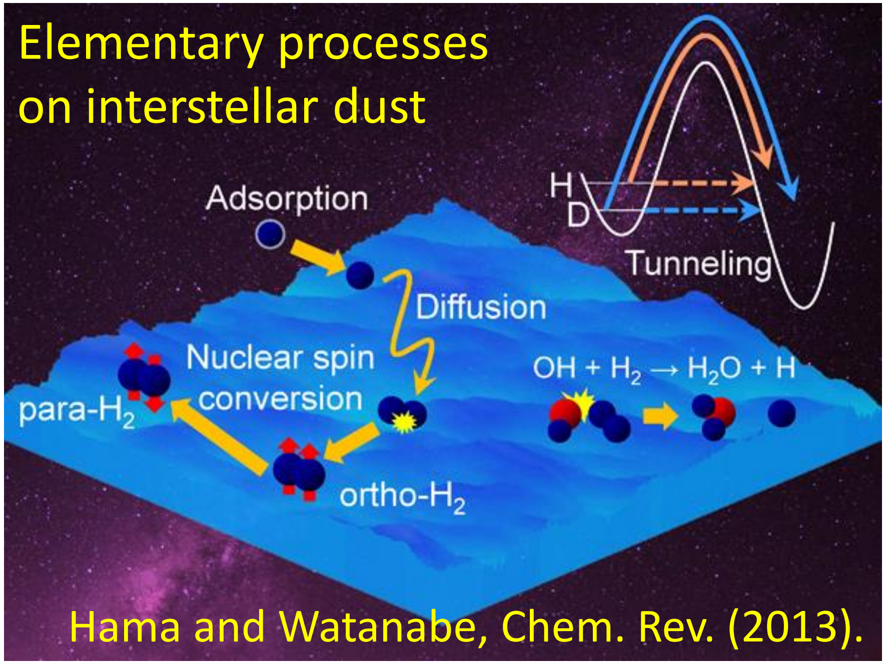

(1) Quantum tunneling surface reactions: H_2CO and CH_3OH formation by H + solid CO

Hama and Watanabe, Chem. Rev. (2013).

(2) Enhancement of H-atom tunneling reactions on amorphous surface.

Hama et al., J. Phys. Chem. Lett. (2014). Hama et al., PNAS (2015).

(3) Photochemistry (photodesorption) of amorphous water ice

Nuclear-spin isomers of photodesorbed H_2O Hama et al., Science (2016)., Astrophys. J. (2018).

Electrical properties of amorphous molecular solids at low temp.

Charge build-up in ice layers condensing on liquid nitrogen traps

When normal atmospheric air is admitted to a vacuum system containing a filled or part-filled liquid nitrogen trap then the condensed ice layer may contain a considerable charge. This phenomenon has been repeatedly observed when admitting air to the UHV system shown in the diagram. Sparks up to 2 cm long have been observed when the lid and trap assembly is lowered towards an earthed surface. To eliminate the risk of electric shock the lid is always earthed by a flexible lead; however, the discharge still occurs. Discharges through the thin ice film have been observed by rocking the trap on a perspex sheet, although arcs from the surface of the ice to an earthed plane through the air is the usual method of discharge. As many as four separate discharges over a space of 10 min have been observed. The mechanism of this charged layer is believed to arise from dissociation of some of the water molecules on condensation. Latham and Mason (1961)[1] have proposed a mechanism for the production of an electrostatic dipole in ice, as part of the mechanism accounting for the charge in thunderclouds. If a temperature gradient exists across a block of ice then there is a greater concentration of H^+ and OH^- at the warmer rather than the cooler end due to thermodynamic dissociation. The more mobile proton diffuses to the cooler end producing an electrostatic dipole. A temperature gradient $\Delta T(K)$ pro-

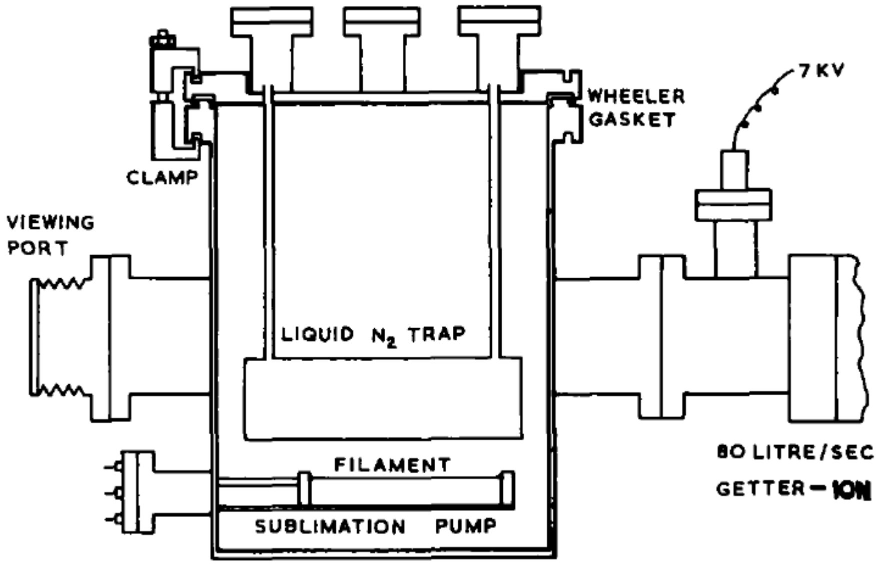

UHV System

disorder is taken up by the dissociation of about one in every 10^5 of the water molecules initially condensing then the subsequent proton diffusion could produce voltages in excess of 50 kV.

It is important for users of vacuum equipment containing liquid nitrogen traps to note that the liquid must be allowed to boil off before admitting atmospheric air. Otherwise one runs the risk of electric shock. Also in some systems there may be a fire risk if volatile inflammable vapours happen to be present.

E Elliott, T I Pritchard, M J Hampshire and R D Tomlinson
Electrical Engineering Department
University of Salford
Salford, Lancs

References

[1] J Latham and B J Mason, *Proc RS A*260, 1961, 537.
[2] J Latham, *Brit J Appl Phys*, **14**, 1963, 488-90.

Molecular orientational order in nanometer-thick films of molecules?

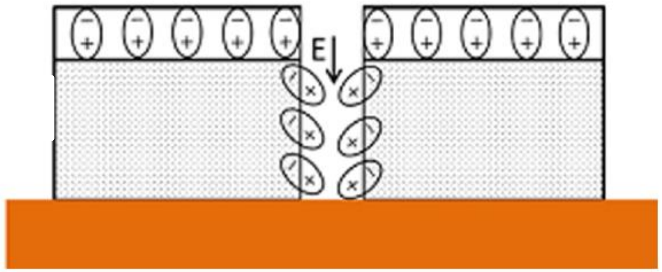

Bu et al., J. Chem. Phys. 2015, 142 (13), 134702.

Elliott et al., Vacuum 1969, 19 (8), 366.

Many polar molecules develop a surface potential during vapor deposition on a cold substrate, e.g., 10^8 V/m for N_2O!

Field et al., Int. Rev. Phys. Chem. 2013, 32, 345.
Plekan et al., Eur. Phys. J. D 2017, 71, 162.

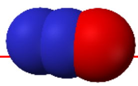

Molecule	Temperature/K	mV/ML	Electric field V/m	Degree of dipole alignment	Gas phase dipole moment/D
Propane	40	−0.72 and −4.77	–	–	0.08
Isopentane	40	−7.8	–	–	0.13
N_2O	40	+32	9.72×10^7	0.124	0.167
Isoprene	40	+35	–	–	0.25
Toluene	40	+6.5	–	–	0.385
CF_3Cl	40	−11.6	-4.25×10^7	0.052	0.500
CF_2Cl_2	45	−3.97	-1.43×10^7	0.042	0.510
$CFCl_3$	43	−1.33	-0.532×10^7	0.031	0.45
Methyl formate	40	5.78	2.21×10^7	0.0185	1.766
Ethyl formate	40	~20 mV/L	–	–	1.98
2,5-Dihydrofuran	40	2.7 mV/L	–	–	1.75

In addition, H_2O, CO, NO, SO_2, NH_3, acetone, propane, and alcohols ($C_nH_{2n+1}OH$, n=1−5).

Dipole alignment in amorphous molecular solid?

Technical difficulties to study molecular orientation in thin films

Diffraction (X-ray, electron, neutron) → Not suitable for amorphous solid

Nuclear magnetic resonance → Low sensitivity for thin films (nm-scale)

Infrared Multiple Angle Incidence Resolution Spectrometry (IR-MAIRS) for molecular orientation analysis developed by Prof. Takeshi Hasegawa (Kyoto Univ.)

Oblique incidence measurements + Multivariate analysis
→ In-plane (IP) and out-of-plane (OP) vibration spectra

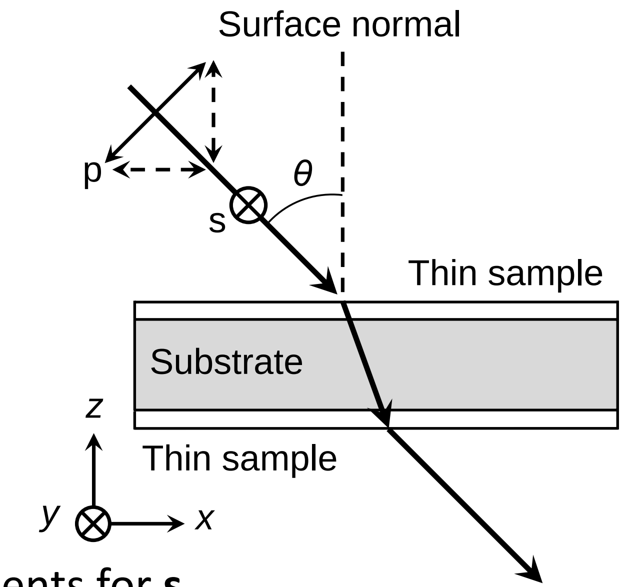

(1) Seven IR spectra are collected at θ=45° with polarization angles (ϕ) from s-pol. (ϕ=0°) to p-pol. (ϕ=90°) in 15° steps.
These spectra ($\mathbf{s}_{\mathrm{obs},\,1\text{-}7}$) are expressed as a linear combination of the IP ($\mathbf{s}_{\mathrm{IP}}$) and OP ($\mathbf{s}_{\mathrm{OP}}$) components

$$\mathbf{s}_{\mathrm{obs},1} = r_{\mathrm{IP},1}\,\mathbf{s}_{\mathrm{IP}} + r_{\mathrm{OP},1}\,\mathbf{s}_{\mathrm{OP}} + \mathbf{u}_1 \text{ (s-pol.)}$$
$$\mathbf{s}_{\mathrm{obs},2} = r_{\mathrm{IP},2}\,\mathbf{s}_{\mathrm{IP}} + r_{\mathrm{OP},2}\,\mathbf{s}_{\mathrm{OP}} + \mathbf{u}_2$$
$$\mathbf{s}_{\mathrm{obs},3} = r_{\mathrm{IP},3}\,\mathbf{s}_{\mathrm{IP}} + r_{\mathrm{OP},3}\,\mathbf{s}_{\mathrm{OP}} + \mathbf{u}_3$$
$$\mathbf{s}_{\mathrm{obs},4} = r_{\mathrm{IP},4}\,\mathbf{s}_{\mathrm{IP}} + r_{\mathrm{OP},4}\,\mathbf{s}_{\mathrm{OP}} + \mathbf{u}_4$$
$$\mathbf{s}_{\mathrm{obs},5} = r_{\mathrm{IP},5}\,\mathbf{s}_{\mathrm{IP}} + r_{\mathrm{OP},5}\,\mathbf{s}_{\mathrm{OP}} + \mathbf{u}_5$$
$$\mathbf{s}_{\mathrm{obs},6} = r_{\mathrm{IP},6}\,\mathbf{s}_{\mathrm{IP}} + r_{\mathrm{OP},6}\,\mathbf{s}_{\mathrm{OP}} + \mathbf{u}_6$$
$$\mathbf{s}_{\mathrm{obs},7} = r_{\mathrm{IP},7}\,\mathbf{s}_{\mathrm{IP}} + r_{\mathrm{OP},7}\,\mathbf{s}_{\mathrm{OP}} + \mathbf{u}_7 \text{ (p-pol.)}$$

$r_{\mathrm{IP},1\text{-}7}$: weighting coefficients for $\mathbf{s}_{\mathrm{IP}}$
$r_{\mathrm{OP},1\text{-}7}$: weighting coefficients for $\mathbf{s}_{\mathrm{OP}}$
$\mathbf{u}_{1\text{-}7}$: Nonlinear noises (e.g., reflected IR light)

Itoh et al., JPC A 2009, 113, 7810.
Shioya et al., JPC A 2019, 123, 7177.

(2) IP and OP spectra are obtained through classical least-squares regression equation.

$$\mathbf{S}_{\mathrm{obs}} = \begin{pmatrix} \mathbf{s}_{\mathrm{obs},1} \\ \mathbf{s}_{\mathrm{obs},2} \\ \vdots \end{pmatrix} = \begin{pmatrix} r_{\mathrm{IP},1} & r_{\mathrm{OP},1} \\ r_{\mathrm{IP},2} & r_{\mathrm{OP},2} \\ \vdots & \vdots \end{pmatrix} \begin{pmatrix} \mathbf{s}_{\mathrm{IP}} \\ \mathbf{s}_{\mathrm{OP}} \end{pmatrix} + \mathbf{U} \equiv \mathbf{R} \begin{pmatrix} \mathbf{s}_{\mathrm{IP}} \\ \mathbf{s}_{\mathrm{OP}} \end{pmatrix} + \mathbf{U}$$

$$\begin{pmatrix} \mathbf{s}_{\mathrm{IP}} \\ \mathbf{s}_{\mathrm{OP}} \end{pmatrix} = (\mathbf{R}^{\mathrm{T}}\mathbf{R})^{-1}\mathbf{R}^{\mathrm{T}}\mathbf{S}_{\mathrm{obs}}$$

IR-MAIRS for hydrogen-terminated Si(111) surface.

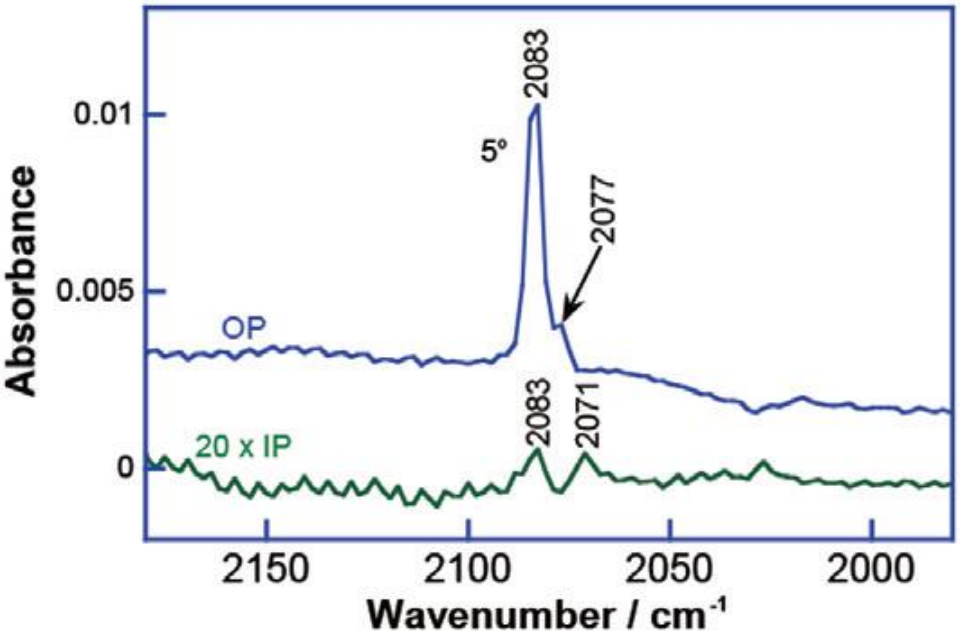

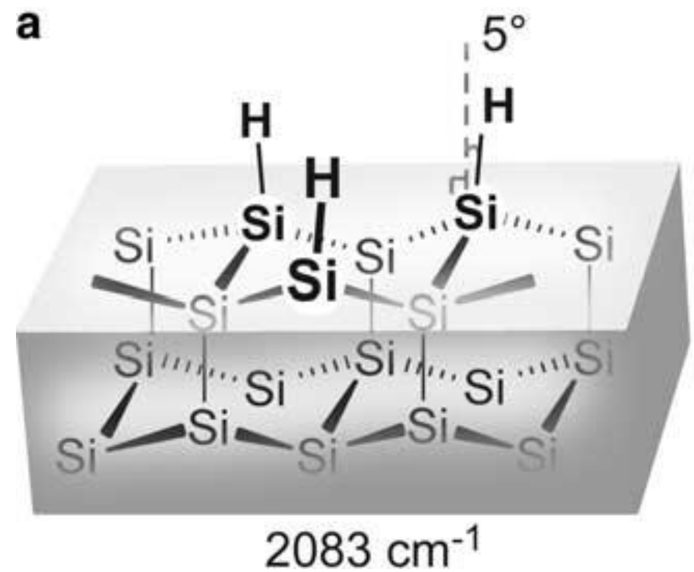

Kakuda et al., Chem. Phys. Lett. 415 (2005) 172.

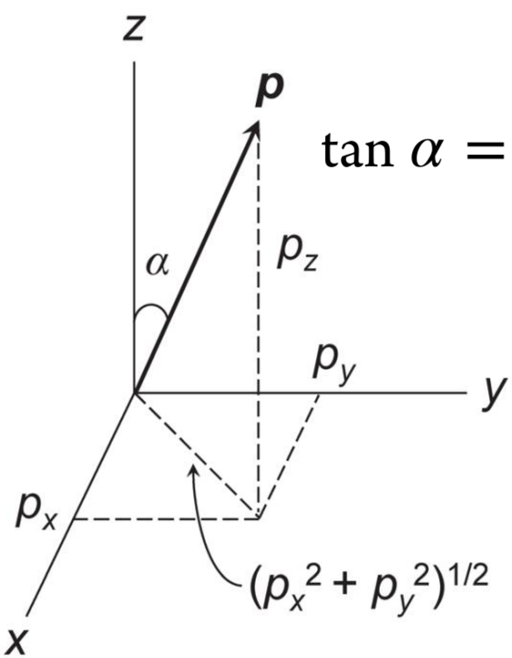

$$\tan\alpha = \frac{\sqrt{p_x^{\ 2} + p_y^{\ 2}}}{p_z} = \frac{\sqrt{2}\,p_x}{p_z} = \sqrt{\frac{2A_{\mathrm{IP}}}{A_{\mathrm{OP}}}}$$

p_i (i = x, y, or z)
x-, y-, and z-components for the transition moment.

(1) High sensitivity to detect one-monolayer
(2) Quantitative molecular orientation analysis
(3) Applicable to amorphous materials

For more details, see Shioya et al., JPC A 2019, 123, 7177.
Hasegawa and Shioya, Bull. Chem. Soc. Jpn. 2020, 93, 1127.

Development of low-temperature, ultrahigh-vacuum IR-MAIRS

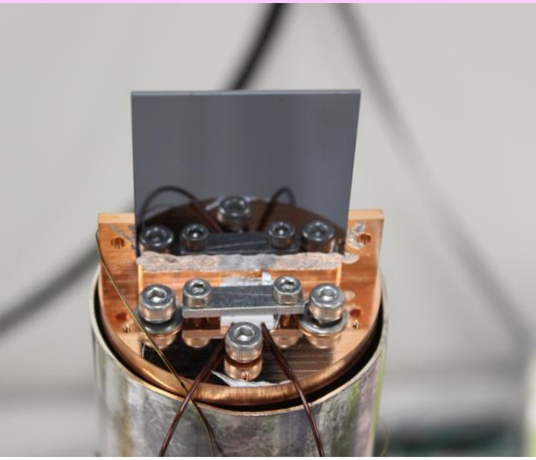

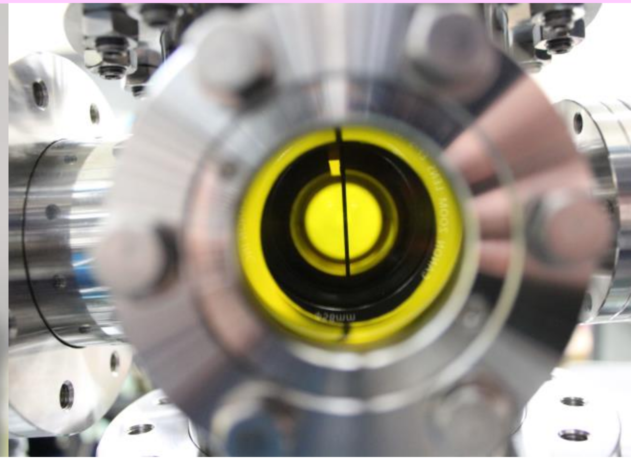

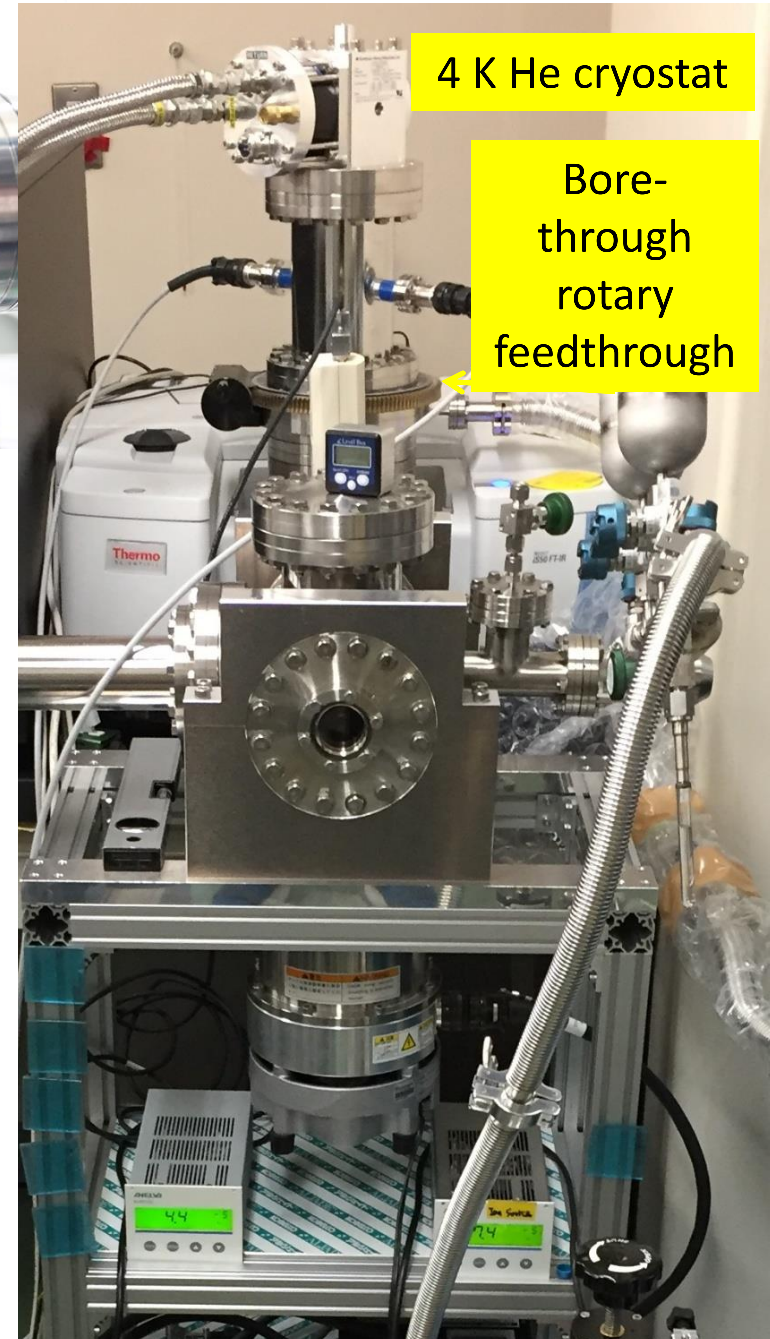

Si(111) substrate and Cu sample holder were connected with indium solder by ultrasonic soldering.

Without thermal shielding, Si can be cooled down to 6 K.

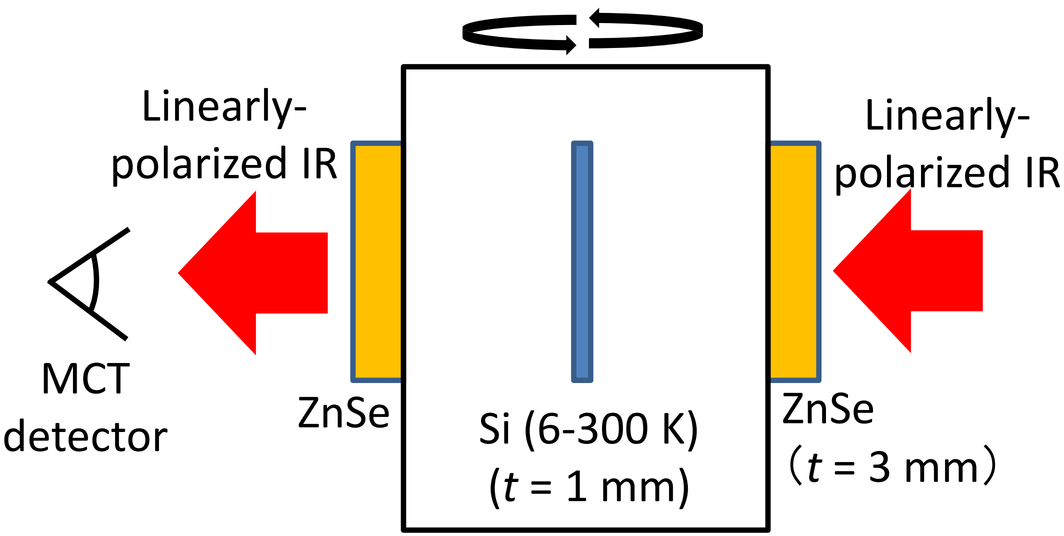

Single-beam spectra measured at various polarization angles from 0° (s-polarization) to 90° (p-polarization) in 15° steps before the MAIRS analysis.

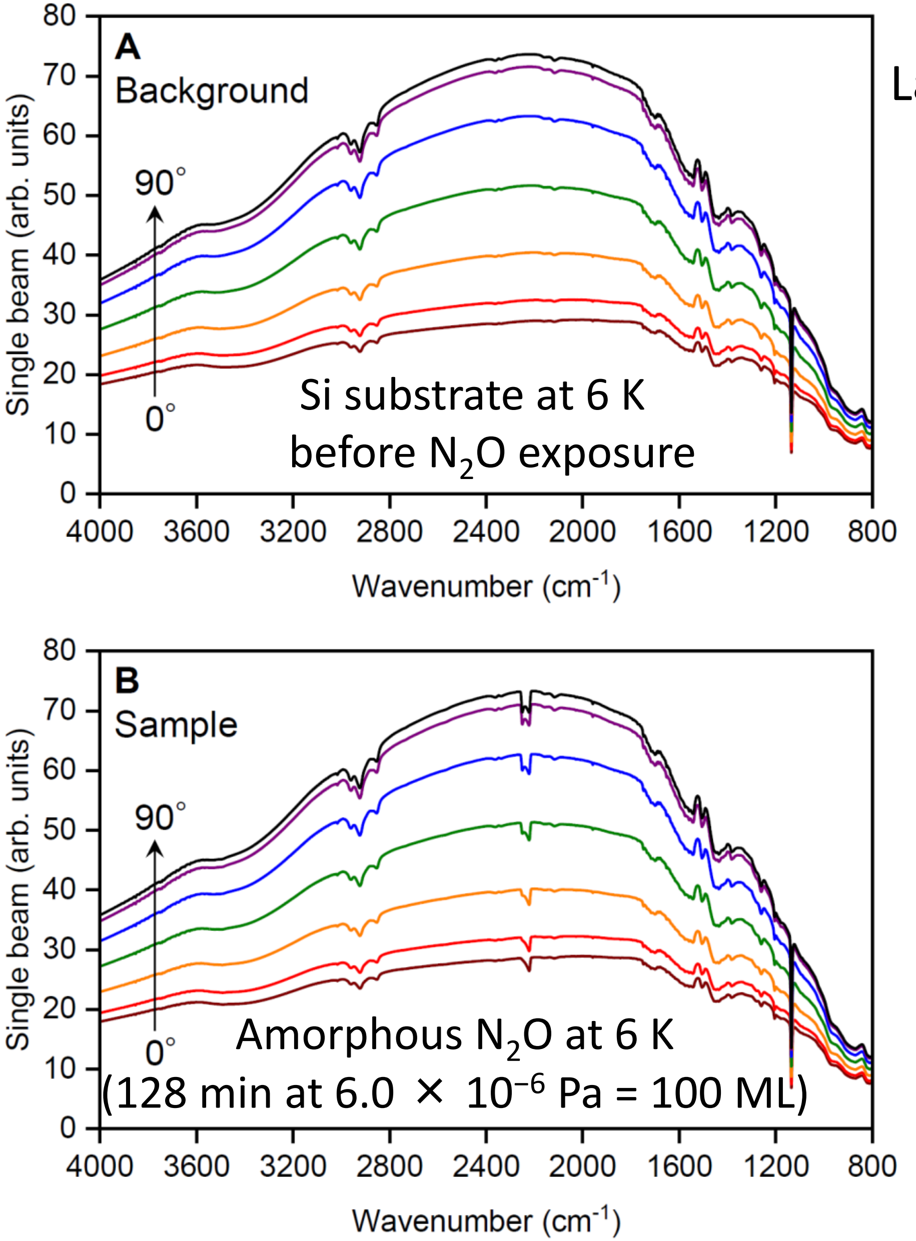

N_2O ($v3$ antisymmetric stretching)

Large TO-LO splitting due to strong absorption

$n + ik$ (n=1.32, k=1.85)

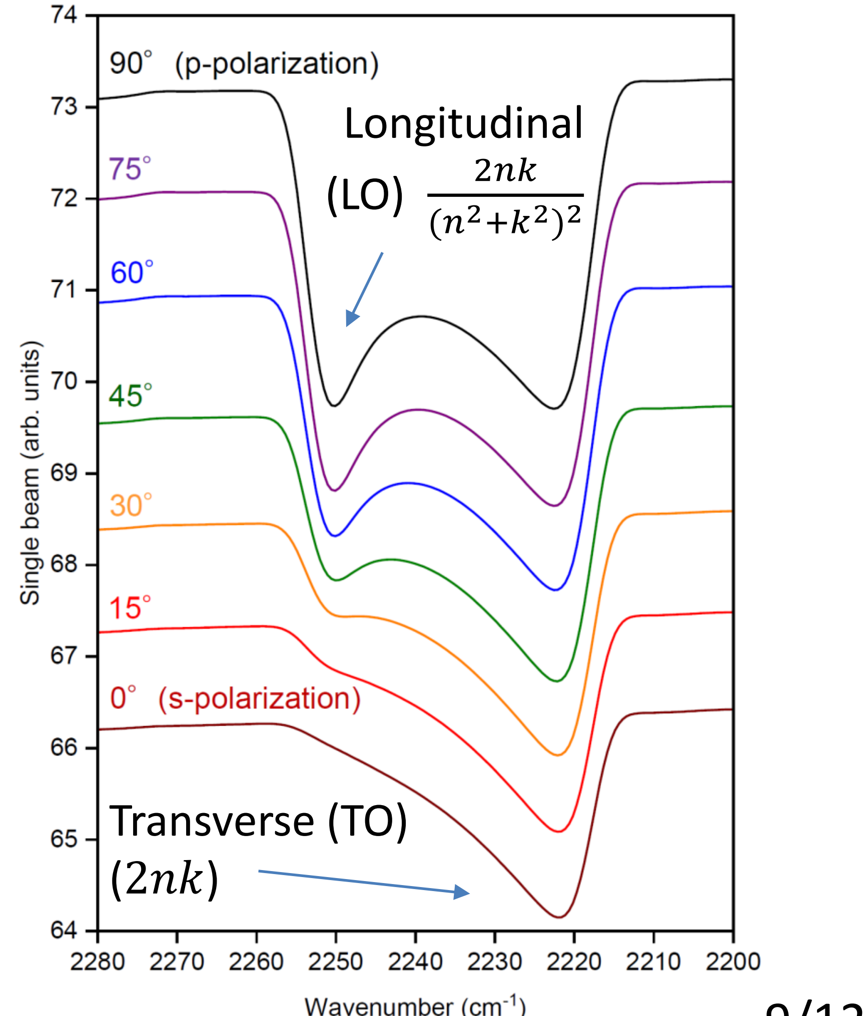

In-plane (IP) spectrum → TO function; Out-of-plane (OP) spectrum → LO function
Large TO-LO splitting in the ν_3 band of $^{14}N^{14}NO$ (n=1.32, k=1.85) is clarified by MAIRS

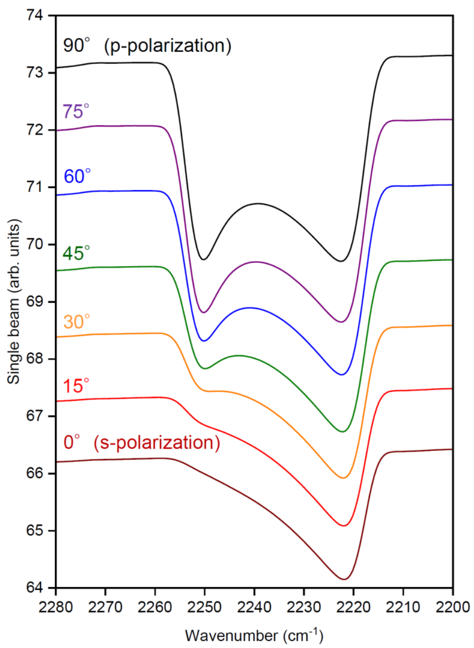

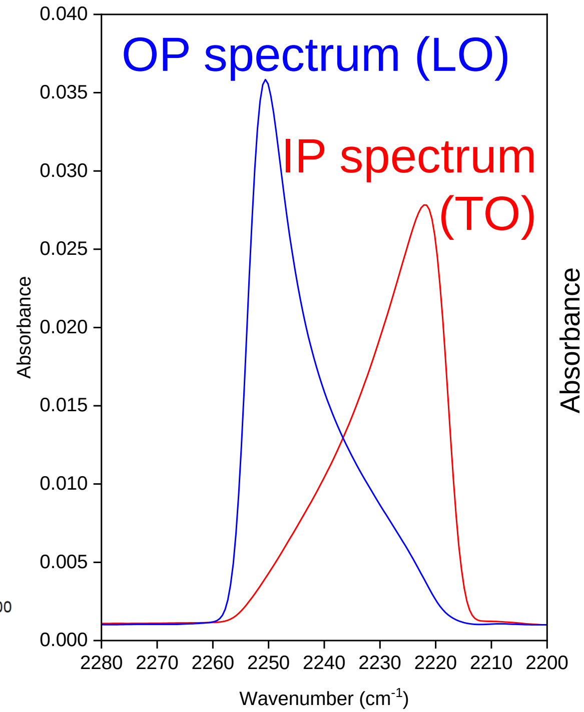

Shioya et al., JPC A 2019, 123, 7177.

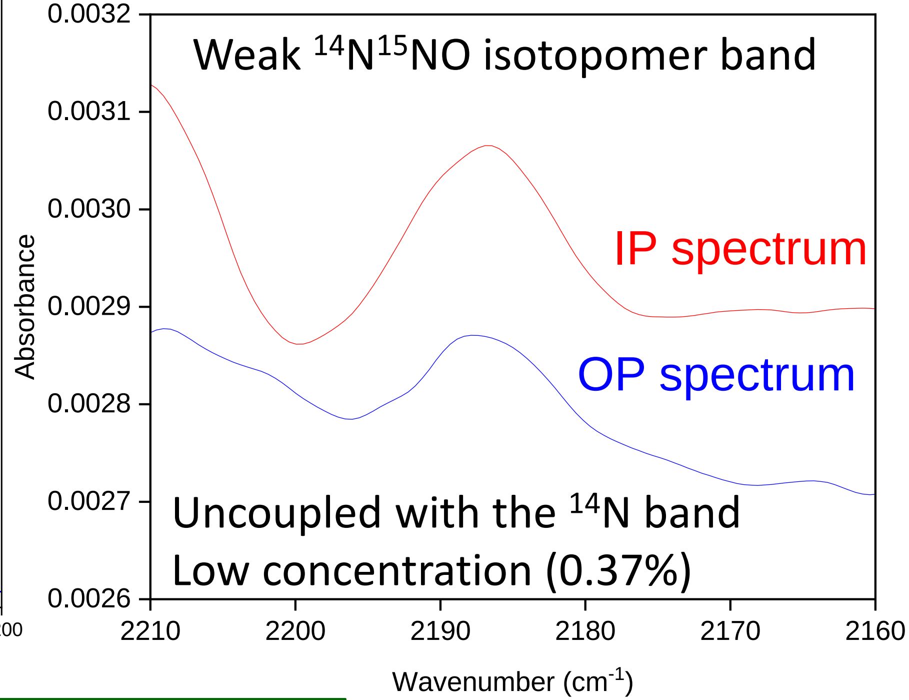

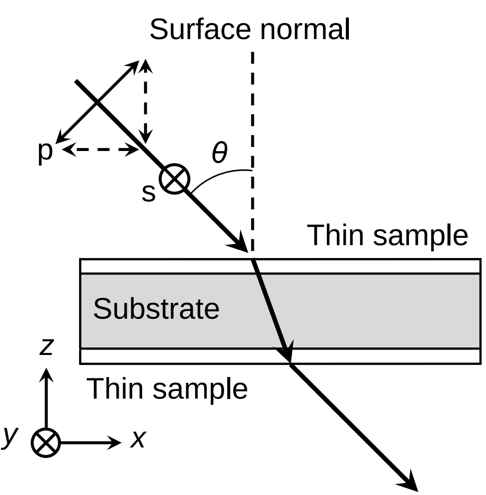

However…. Large TO-LO splitting means
The *v*3 band are delocalized by dipole–dipole interactions between the vibrations of the molecules.
Ovchinnikov and Wight, JCP (1995).
↓
Molecular orientation analysis based on the strong v3 band is inappropriate.

Localized vibration (No TO-LO splitting)
↓
Transition moment direction reflects the molecular orientation

The $^{14}N^{15}NO$ isotope band at 6 K as a function of exposure time

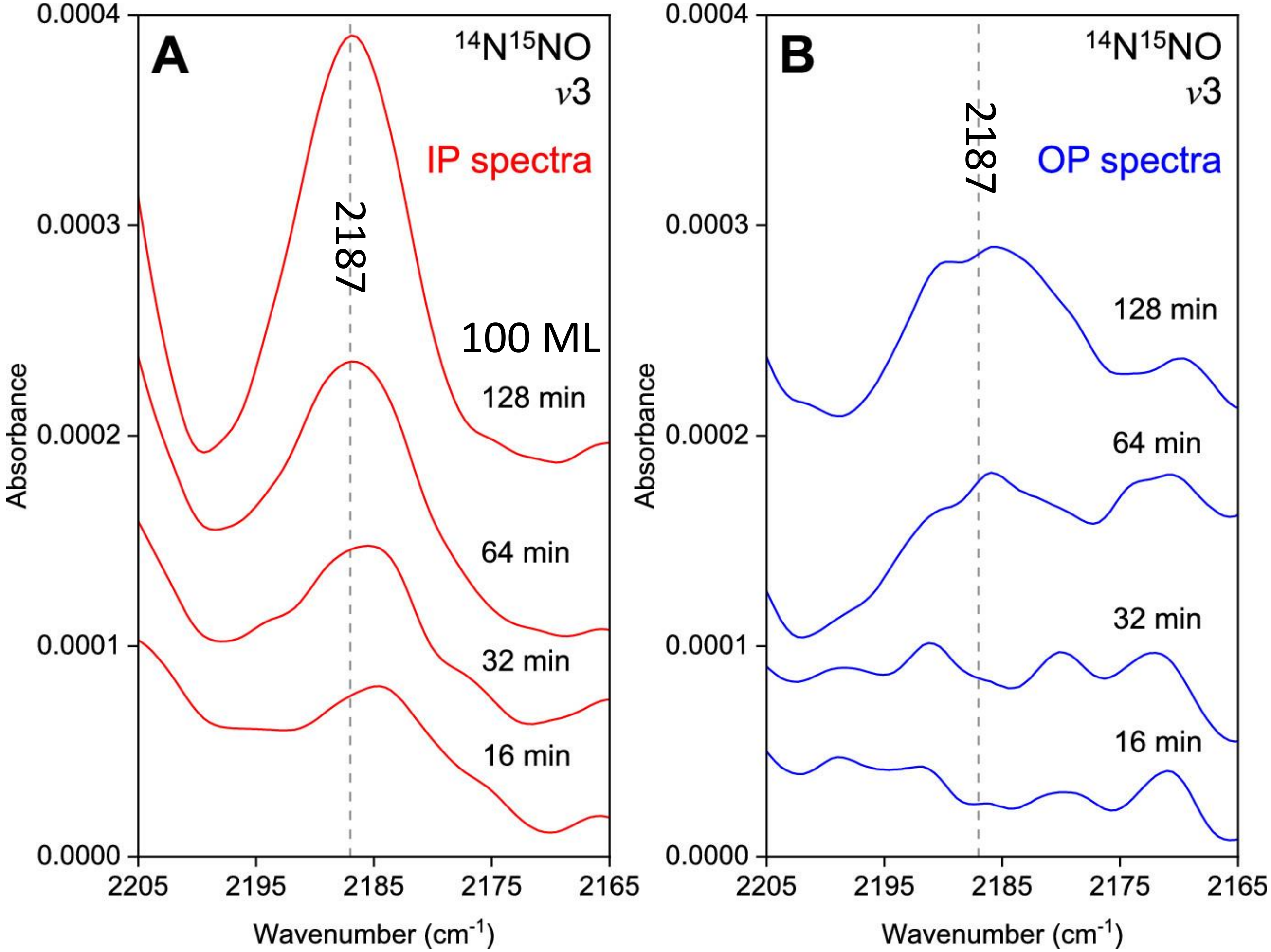

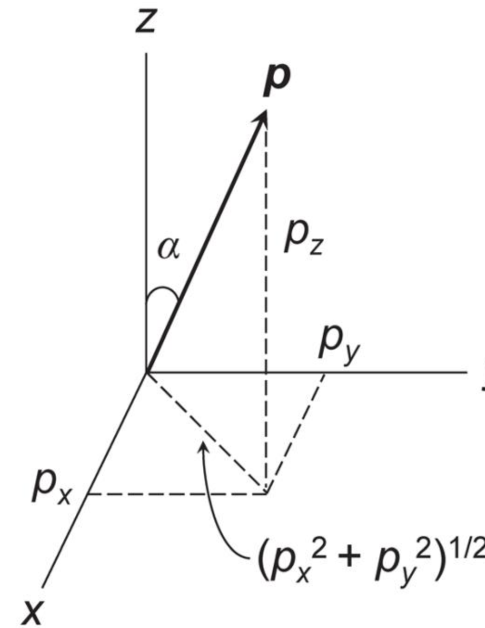

IP > OP
（65.1° ± 1.5° ）

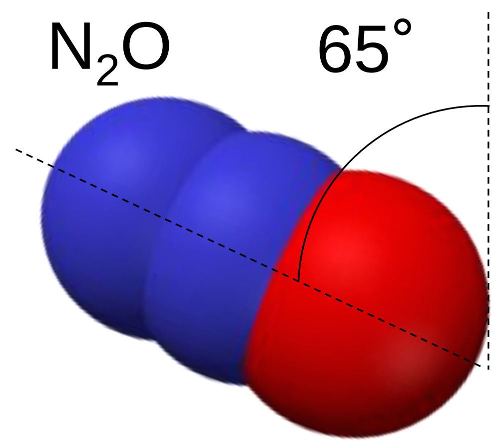

$$\tan\alpha = \frac{\sqrt{p_x{}^2 + p_y{}^2}}{p_z} = \frac{\sqrt{2}\,p_x}{p_z} = \sqrt{\frac{2A_{IP}}{A_{OP}}}$$

IP/OP spectra of amorphous H_2O at 10 K: Dangling-OH bands (2-, and 3-coordinated molecules at the surface)

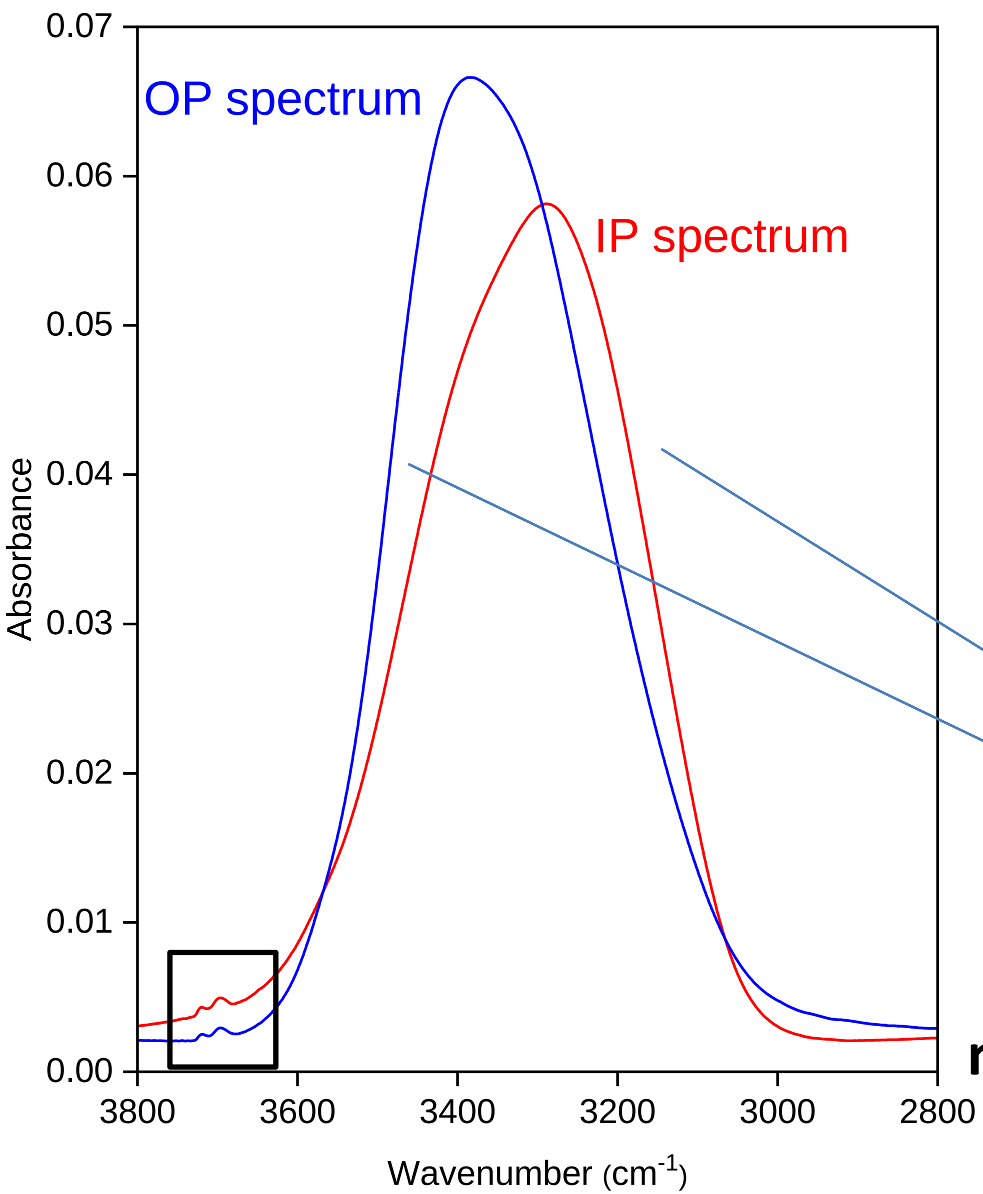

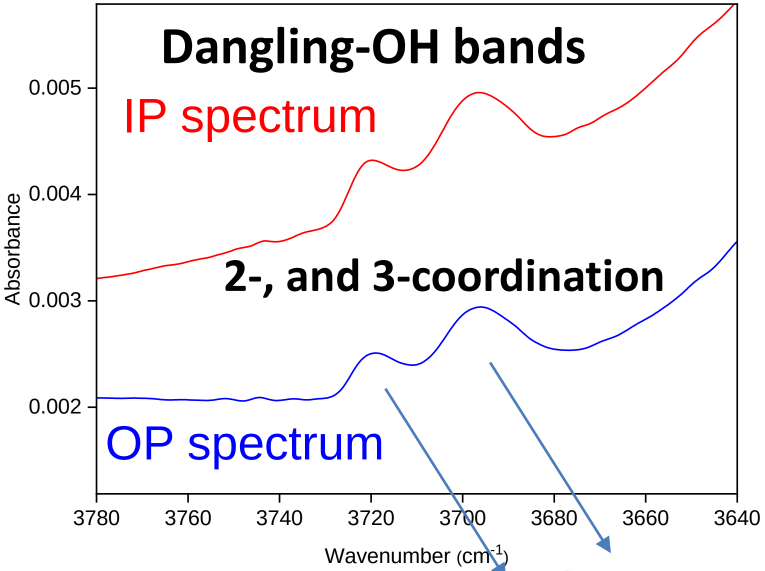

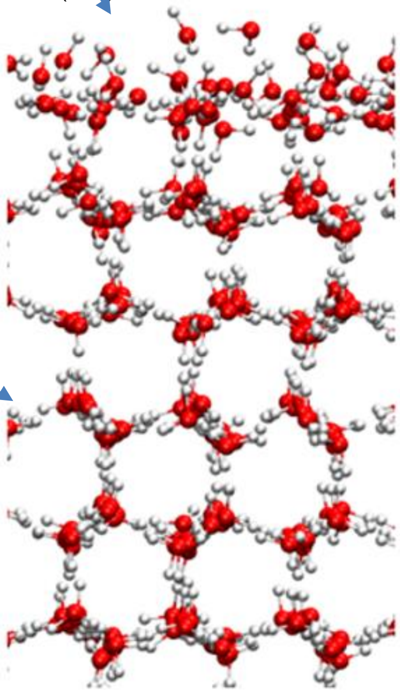

4-coordinated molecules in bulk

Discussion and Summary

(1) Development of low-temperature, ultrahigh vacuum IR-MAIRS

Hama et al., J. Phys. Chem. Lett. 2020, 11, 7857.

(2) Large TO-LO splitting in the *v*3 band of $^{14}N^{14}NO$ in amorphous N_2O at 6 K.

The *v*3 band are delocalized by long-range dipole−dipole interactions (*n*=1.32, *k*=1.85).

→ Inappropriate for molecular orientation analysis.

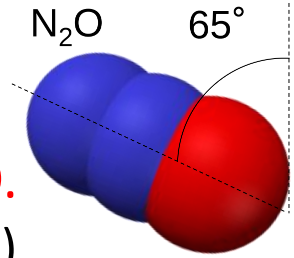

(3) Molecular orientation analysis by the weak *v*3 band of $^{14}N^{15}NO$.

The degree of dipole alignment at 6 K → 0.02−0.03 ($1.6–2.4 \times 10^7$ V m^{-1})

Kutzner, Thin Solid Films 1972, 14, 49.

Orientation angle of 65° ± 2° → 0.42 (Too large!)

The cancellation of the N_2O dipole moments occurs on a macroscopic scale in amorphous N_2O.

The origin of the orientation angle (65°) is unclear.

→ Anisotropy of the van der Waals interactions?

(4) Applicable to interstellar chemistry and other research fields.

e.g., organic semiconductor films.

Pentacene